Functional & Integrative Genomics (2026) 26:150
https://doi.org/10.1007/s10142-026-01917-w

RESEARCH

Deciphering the potential molecular network underlying nicotine- and its metabolite cotinine-induced myocardial infarction via network toxicology, molecular dynamics, and in vitro experimental validation

Yang Fu[1] · Chen Liu[1] · Lifang Su[1]

Received: 1 March 2026 / Revised: 20 May 2026 / Accepted: 29 May 2026

Abstract

Smoking is a major modifiable risk factor for myocardial infarction (MI); however, the molecular mechanisms through which its core component nicotine and its primary metabolite cotinine mediate MI development remain incompletely understood. This study aimed to identify key molecular targets and characterize the mechanistic basis by which nicotine and cotinine mediate myocardial injury relevant to MI. To this end, we performed two-sample Mendelian randomization using GWAS data for smoking (468,170 participants) and MI (20,197 cases, 440,906 controls) from the IEU Open GWAS Project to genetically validate the smoking-MI causal association. Potential targets of nicotine and cotinine were predicted from four databases (SEA, TargetNET, SwissTargetPrediction, ChEMBL). MI-related targets were retrieved from DisGeNET and GeneCards. Shared targets among nicotine, cotinine, and MI were identified, followed by PPI network analysis, GO/KEGG enrichment, and topological screening (MCC and Degree). Core targets were validated using GEO transcriptomic datasets (GSE113871, GSE115031). Molecular docking and 200-ns molecular dynamics simulations were performed to evaluate potential ligand-target interactions. In vitro CCK-8 and qRT-PCR assays in H9c2 cardiomyocytes assessed cytotoxicity and target expression. MR analysis confirmed a significant positive causal association between smoking and MI. We identified 44 shared targets, with ADRA2A validated as the key functional target. Molecular docking suggested that nicotine and cotinine may potentially bind to ADRA2A, with calculated affinities of −7.2 and −6.8 kcal/mol, respectively. MD simulations indicated that the complexes might remain stable during the simulation trajectory. Nicotine and cotinine exerted cytotoxicity in H9c2 cells and significantly upregulated Adra2a mRNA. Collectively, these findings suggest that ADRA2A is a potential critical molecular target mediating nicotine- and cotinine-induced MI, providing novel mechanistic insights and potential therapeutic targets for smoking-related cardiovascular diseases.

Keywords Myocardial infarction (MI) · Smoking · Nicotine · Cotinine · Network toxicology

Background

Myocardial infarction (MI), the most severe subtype of acute coronary syndrome, remains one of the leading causes of cardiovascular mortality worldwide. Its high incidence, recurrence, and disability rates constitute a major public health challenge (Liu and Yang 2025). Among the numerous risk factors for MI, modifiable factors such as smoking, hypertension, diabetes mellitus, and obesity play a substantial role in disease onset (Bujnova et al. 2025, Johansson et al. 2025, Cojocaru et al. 2025). Smoking, in particular, is the second most important independent risk factor after obesity (Ockene and Miller 1997). According to the Global Burden of Disease (GBD) 2021 study, smoking is responsible for approximately 3 million deaths globally. In addition to active smoking, exposure to secondhand smoke significantly increases the risk of MI, while thirdhand smoke residues—defined as the long-term deposition of nicotine and its metabolites on environmental surfaces—further expand

Yang Fu is a first author.

✉ Yang Fu
fuyang@hebmu.edu.cn

[1] Department of Cardiology, The Second Hospital of Hebei Medical University, Shijiazhuang 050000, Hebei, China

Published online: 19 June 2026

the population exposed to tobacco-related toxins (Ockene and Miller 1997, Rosa et al. 2025).

Although extensive epidemiological evidence has established a strong association between smoking and MI, the underlying molecular mechanisms remain incompletely understood (Yathindra et al. 2025, Hu et al. 2025). Previous studies have shown that smoking-induced myocardial injury may involve oxidative stress, inflammatory activation, dysregulation of the α7 nicotinic acetylcholine receptor (α7nAChR) signaling pathway, and calcium homeostasis imbalance (Klein et al. 2023, Kumar and Biswas 2011, Lee et al. 2017). For example, a recent animal study reported that chronic exposure to tobacco smoke prior to myocardial infarction exacerbates myocardial necrosis and leads to worse cardiac function, a finding closely associated with elevated transcriptional levels of pro-inflammatory cytokines, tissue repair molecules, and oxidative stress markers in myocardial tissue (Khanna et al. 2012). However, most of these studies have focused on single molecules or individual pathways, lacking a systematic, multi-target network-level analysis of the molecular mechanisms underlying smoking-related myocardial injury.

Nicotine, the principal bioactive component of tobacco, has been designated as a "priority environmental pollutant" by both the U.S. Environmental Protection Agency (EPA) and the World Health Organization (WHO) (Ghanem et al. 2026). Nicotine enters the human body not only through active smoking but also via secondhand smoke aerosols and thirdhand smoke adsorbed onto indoor surfaces such as walls, furniture, and clothing, creating persistent environmental exposure sources. Consequently, non-smokers may passively absorb nicotine through inhalation or dermal contact (Patil et al. 2025, Sasco et al. 2004). Cotinine, the primary metabolite of nicotine, similarly exhibits environmental pollutant characteristics and has been widely detected in indoor dust, drinking water, and airborne particulate matter in public spaces. Owing to its high stability, cotinine is widely recognized as a reliable biomarker for assessing environmental nicotine exposure (Sahin et al. 2026, Riederer et al. 2025).

Studies have confirmed that nicotine acts directly on myocardial tissue, inducing cardiomyocyte injury, apoptosis, enhanced oxidative stress, and abnormal cardiac remodeling, thereby contributing to the pathological process of MI (Baykan et al. 2008, Hanna 2006, Meng et al. 2021, Jia et al. 2020, Ramalingam et al. 2021). In addition, nicotine promotes the development and progression of coronary artery disease and MI through multiple pathways, including coronary artery spasm, myocardial ischemia, and arrhythmias (Balakumar and Kaur 2009). Animal studies further demonstrate that chronic nicotine exposure prior to MI significantly increases infarct size, and continued exposure after MI further enlarges the infarct area (Sridharan et al. 1985). Although research on the direct myocardial toxicity of cotinine is relatively limited, as a persistent environmental metabolite of nicotine, it may still affect myocardial homeostasis through similar or independent mechanisms. Previous studies suggest that even low-level exposure to environmental nicotine and cotinine may disrupt cardiovascular homeostasis. However, as molecular mediators with dual identities as both cigarette constituents and environmental pollutants, their specific targets, downstream signaling pathways, and mechanistic roles in MI pathogenesis have yet to be systematically elucidated.

To fill this gap, the present study adopted a stepwise, multi-level strategy. First, two-sample Mendelian randomization (MR) was employed to genetically validate the causal association between smoking behavior and MI, using genetic variants as instrumental variables to minimize confounding bias and reverse causation inherent in observational studies. This provides a robust population-level causal foundation for subsequent mechanistic investigations. Second, network toxicology—an interdisciplinary approach integrating computational biology, toxicology, and systems biology—was applied to systematically predict multi-target and multi-pathway interactions of nicotine and cotinine with the human proteome through high-throughput target prediction, functional enrichment analysis, and network construction (Dasgupta 2024, Yuan et al. 2025, Cheng et al. 2026). This step identifies the potential molecular targets linking these compounds to MI. Finally, to experimentally validate the computational findings, the H9c2 cardiomyocyte line, a classic model for myocardial toxicity validation, was selected for in vitro assays (Rao et al. 2024, Wu et al. 2023). Thus, this study forms a coherent research pipeline that progresses from population causal inference (MR) to molecular target screening (network toxicology) and then to biological validation (cell experiments).

By integrating Mendelian randomization, network toxicology, transcriptomic analysis, and molecular biology experiments, this study aims to genetically confirm the causal link between smoking and MI, and to systematically identify the key molecular targets and mechanisms through which nicotine and cotinine mediate myocardial injury relevant to MI. It should be noted that this study does not simulate overall exposure to third-hand smoke, but rather focuses on its core toxic components—nicotine and cotinine. Whether these two molecules originate from active smoking or passive environmental exposure, their key toxic mechanisms may share common features. Therefore, the findings of this study are expected to be applicable to both the effects of smoking itself and environmental exposure scenarios. We anticipate that these findings will provide a theoretical basis and potential intervention targets for the prevention and treatment of smoking-related myocardial infarction.

Materials and methods

Mendelian randomization analysis

Summary-level GWAS data for the exposure factor (smoking status) was obtained from the IEU Open GWAS Project database (GWAS ID: ebi-a-GCST90029014), which includes 468,170 European participants and 1,197,342 SNPs. The summary-level GWAS data for the outcome (myocardial infarction, MI) was also sourced from the IEU Open GWAS Project (GWAS ID: ebi-a-GCST90018877), comprising 20,197 MI cases and 440,906 controls, involving 24,172,914 SNPs, with the same European population. These datasets contain core information, including effect sizes, standard errors, and P-values, and all participants were of European ancestry to minimize bias from race, geography, and other potential confounders.

Instrumental variables (IVs) were selected following strict criteria: genome-wide significance threshold was set at $P < 5 \times 10^{-8}$, and variants with MAF < 0.01 were excluded (Lou et al. 2024). Linkage disequilibrium (LD) analysis ($r^2 < 0.001$, window size = 10,000 kb) was employed to remove redundant variants, while ensuring no significant population stratification. After filtering, the remaining genetic instruments met the inclusion criteria for causal effect estimation. To minimize the risk of weak instrument bias, variants with an F-statistic below the conventional threshold of 10 were excluded. LD Link (https://ldlink.nih.gov/) was used to assess and exclude potential pleiotropic SNPs.

For the analysis, effect alleles for both the exposure and outcome datasets were harmonized, and palindromic sequences were removed. The analysis was performed using R 4.2.0 software with the TwoSampleMR package, utilizing the inverse variance weighted (IVW) method (primary analysis), along with MR-Egger regression, weighted median, simple model, and weighted mode methods for causal effect estimation (Sanderson et al. 2022, Bowden et al. 2015, Bowden et al. 2016). The IVW method assumes all instruments are valid and provides the weighted average effect size using inverse variance weighting, thereby improving precision under core assumptions. Therefore, IVW was chosen as the primary method, with the other four methods as supplementary analyses.

Sensitivity analysis

Sensitivity analyses were conducted using the TwoSampleMR package in R 4.2.0 to assess the reliability of the results. The analyses included leave-one-out sensitivity analysis, MR-Egger intercept test, heterogeneity test, and funnel plot analysis. In the leave-one-out analysis, each genetic instrument was sequentially excluded, and the IVW analysis was rerun to observe any changes in the effect size and determine the influence of individual instruments on the overall result. The MR-Egger intercept test was used to assess horizontal pleiotropy, with a P-value ≥ 0.05 indicating no significant pleiotropy. Funnel plot analysis was employed to examine the symmetry of effect estimates, ensuring the stability and reliability of the Mendelian randomization results.

To further evaluate the robustness of the results, we assessed heterogeneity and pleiotropy in the instrumental variables. Cochran's Q test was used to assess heterogeneity; a P-value < 0.05 indicates significant heterogeneity (Greco et al. 2015). MR-Egger intercept test was used to evaluate horizontal pleiotropy, with $P < 0.05$ indicating the presence of significant pleiotropy (Chen et al. 2020). Additionally, the MR-PRESSO method was used to identify outliers among the instruments, and outlier removal was performed to correct for any potential biases (Verbanck et al. 2018). Finally, the leave-one-out analysis was conducted to assess the stability of the results (Corbin et al. 2016).

Prediction of potential targets for nicotine and cotinine

The molecular structures of nicotine (PubChem CID: 89594) and cotinine (PubChem CID: 854019) were downloaded from the PubChem database (https://pubchem.ncbi.nlm.nih.gov/) in SDF format to ensure the structures were free from redundant atoms or bonds. High-throughput target prediction was performed using four databases: SEA (https://sea.bkslab.org/), TargetNET (http://targetnet.scbdd.com/), SwissTargetPrediction (http://www.swisstargetprediction.ch/), and ChEMBL (https://www.ebi.ac.uk/chembl/) (Nowotka et al. 2017, Yao et al. 2016). For each database, predictions were filtered using the recommended confidence thresholds to exclude low-confidence and spurious entries, and all predictions were restricted to Homo sapiens. The results from each database were aggregated, and target protein names were standardized to gene symbols using the UniProt database (https://www.uniprot.org/). Duplicate entries, non-protein-coding targets, and low-confidence false positive candidates were sequentially removed to minimize prediction noise. After strict filtering, a high-confidence set of potential targets for nicotine and cotinine was obtained.

Identification of myocardial infarction targets

MI-related targets were retrieved from two disease-target databases: DisGeNET (https://www.disgenet.org/) and GeneCards (https://www.genecards.org/) (Stelzer et al. 2016). For the DisGeNET database, the keyword "Myocardial

Infarction" was used, and targets with a GDA (Gene–Disease Association) score > 0.3 were selected. For the GeneCards database, the same keyword was used; targets were ranked by Relevance score in descending order, and the top 50% were retained. The targets from both databases were aggregated, and duplicates were removed to obtain a core myocardial infarction (MI)-related target set, which served as the foundation for subsequent intersection analysis.

Functional enrichment analysis

Functional and pathway enrichment analyses were performed using the ClusterProfiler package in R 4.2.0 for the following sets: "Nicotine-Cotinine Intersection Targets" and "Nicotine-Cotinine-MI Intersection Targets." These analyses included Gene Ontology (GO) enrichment analysis (covering biological processes, molecular functions, and cellular components), Kyoto Encyclopedia of Genes and Genomes (KEGG) pathway enrichment, and Reactome pathway analysis. All enrichment analyses were filtered with corrected $P < 0.05$ and false discovery rate (FDR) < 0.05. The results were visualized using bubble plots and bar charts generated by the ggplot2 package to provide a clear understanding of the functional characteristics and core pathways involved.

Core target selection

Venn diagrams were drawn using Venny 2.1 (https://bioinfogp.cnb.csic.es/tools/venny/) to identify the intersection of nicotine potential targets, cotinine potential targets, and MI-related targets. The intersection targets were imported into the STRING database (https://string-db.org/), with a minimum interaction score ≥ 0.7, and isolated nodes with no interactions were excluded (Szklarczyk et al. 2015). The protein-protein interaction (PPI) network data was exported. Cytoscape 3.9.1 (https://cytoscape.org/) was used for visualization of the PPI network. The MCC (Maximum Clique Centrality) and DEGREE algorithms were applied using the CytoHubba plugin to identify core targets, and the intersection of both algorithms was used as the core set of targets mediating the effects of nicotine and cotinine on MI.

Transcriptomic analysis

MI-related transcriptomic data sets (GSE113871 and GSE115031) were downloaded from the GEO database (https://www.ncbi.nlm.nih.gov/geo/). The GSE113871 dataset includes 3 MI samples and 3 normal control samples, and GSE115031 includes 3 MI samples and 3 normal control samples, both consisting of mRNA expression profiles. The raw data was normalized using the limma package in R 4.2.0, which included background correction and normalization. Box plots were used to verify the normalization. UMAP (Uniform Manifold Approximation and Projection) was used to visualize clustering of MI and normal control samples, ensuring clear sample phenotype distinction. Differential expression analysis was performed using the limma package, with a threshold of $|\log_2(\text{Fold Change})| \geq 1$ and adjusted $P < 0.05$. Volcano plots were generated to visualize differentially expressed genes, and the expression characteristics of core targets were validated.

Molecular docking

The initial high-resolution crystal structure of human ADRA2A (PDB ID: 6KUX, resolution 2.70 Å) was retrieved from the RCSB PDB (https://www.rcsb.org/). Missing atoms and residues in the protein structure were repaired using PDBfixer (https://github.com/openmm/pdbfixer) to ensure structural integrity. The SDF files of nicotine (PubChem CID: 89594) and cotinine (PubChem CID: 854019) were imported into PyMOL 2.5 software for redundant structure removal and conformational optimization. AutoDockTools 1.5.6 was used to add hydrogens, calculate Gasteiger charges, and convert the ligands into PDBQT format. Molecular docking was performed using AutoDock Vina software. The active pocket of ADRA2A was defined via PyMOL 2.5, and a grid box (60 × 60 × 60 Å) with a grid point spacing of 0.375 Å was set to fully enclose the binding site. The conformation with the lowest binding free energy was selected as the optimal binding mode. Interactions between ligands and ADRA2A were visualized using PyMOL 2.5.

Molecular dynamics simulation

Molecular dynamics (MD) simulations of the optimal "Nicotine-ADRA2A" and "Cotinine-ADRA2A" complexes were performed using GROMACS 2021.4. The protein was parameterized with the AMBER ff14SB force field, while the GAFF force field was used for ligand parameterization. Atomic partial charges of nicotine and cotinine were derived using the RESP2 scheme based on quantum chemical calculations (ORCA 5.0.3 for geometry optimization and frequency analysis; Multiwfn 3.8 for RESP2 charge fitting) to ensure high accuracy of ligand electrostatic properties. Each complex was placed in a periodic cubic water box and solvated with the TIP3P water model, and sodium ions were added to neutralize the system charge. Energy minimization was performed using the steepest descent algorithm (50,000 steps) to eliminate spatial steric clashes, followed by conjugate gradient minimization until the maximum force was lower than 100 kJ/(mol·nm). NVT equilibration (100 ps, 300 K) and NPT equilibration (100 ps, 1 bar) were

sequentially conducted using the V-rescale thermostat and Parrinello-Rahman barostat (relaxation time τp = 2.0 ps, compressibility = 4.5×10^{-5} bar^{-1}) to maintain temperature and pressure stability. Separate temperature coupling groups were applied to the protein-ligand complex and the solvent. Three independent 200 ns NPT production simulations were performed without restraints, with trajectory files saved every 10 ps. A cutoff of 10 Å was applied for van der Waals and short-range electrostatic interactions, while long-range electrostatics were treated using the particle mesh Ewald (PME) method. A time step of 2 fs was used throughout all simulations. All simulations were conducted on an NVIDIA GeForce RTX 4090 GPU with a 24-core CPU. Trajectory analyses included root mean square deviation (RMSD), root mean square fluctuation (RMSF), radius of gyration (Rg), solvent-accessible surface area (SASA), and hydrogen bond occupancy, which were performed using GROMACS tools, VMD, and Grace software.

CCK-8 assay

H9c2 cardiomyocytes were obtained from the ATCC cell bank (USA) and cultured in DMEM high-glucose medium (Thermo Fisher) containing 10% fetal bovine serum (Gibco) and 1% penicillin-streptomycin (Sigma), maintained at 37 °C with 5% CO_2. The cells were subcultured when reaching 80% confluence. The experimental groups included control and nicotine/cotinine treatment groups, with three replicates per group. H9c2 cells were seeded at a density of 5×10^3 cells/well in a 96-well plate and cultured for 72 h. The medium was replaced with medium containing different concentrations of nicotine or cotinine (1, 5, 10, 20, 40, 50, 100, and 200 μM) and cultured for another 72 h. Notably, the highest concentration (200 μM) was used exclusively for constructing a complete dose–response curve and calculating IC_{50} values, and was not applied in subsequent mechanistic experiments. 10 μL of CCK-8 reagent (Beyotime) was added to each well and incubated for 2 h at 37 °C. Absorbance at 450 nm was measured using a microplate reader (Bio-Rad). Cell viability was calculated as follows: Cell viability = (OD of treatment group / OD of control group) × 100%. The concentration-cell viability curve was plotted using GraphPad Prism 8.0.2, and the half-maximal inhibitory concentration (IC_{50}) of nicotine and cotinine on H9c2 cells was determined by nonlinear regression fitting.

qRT-PCR

Total RNA from H9c2 cells in each group was extracted using TRIzol reagent (Invitrogen) according to the manufacturer's instructions. RNA purity (A260/A280 = 1.8 ~ 2.0) and concentration were determined using a Nanodrop 2000 spectrophotometer to ensure RNA integrity. Reverse transcription was performed using the PrimeScript RT reagent kit (TaKaRa) in a 20 μL reaction volume, with 1 μg total RNA as template. The reaction conditions were 37 °C for 15 min, 85 °C for 5 s, followed by storage at 4 °C. cDNA was used as a template for quantitative PCR using the SYBR Green PCR kit (TaKaRa). *β-ACTIN* was used as the reference gene. The primer sequences for *Adra2a* were 5′- TTG GTAAGGTGTGGTGCGAG − 3′ (forward) and − 5′- CCTG CGTGATGGACCAGTAG − 3′ (reverse). The β-actin primers were 5′- CCCATCTATGAGGGTTACGC − 3′ (forward) and 5′- TTTAATGTCACGCACGATTTC − 3′(reverse). For qRT-PCR analysis, cells were treated with 10 μM nicotine or cotinine. At this concentration, cell viability was only slightly decreased with no obvious cell death, ensuring that the observed changes in *Adra2a* expression represented specific biological responses rather than non-specific cytotoxicity. PCR reactions were performed with a 20 μL total volume, containing 10 μL 2×SYBR Premix Ex Taq II, 0.4 μL of each primer (10 μM), 2 μL cDNA, and 7.2 μL RNase-free water. The PCR conditions were 95 °C for 30 s, followed by 40 cycles of 95 °C for 5 s, 60 °C for 30 s. Melting curve analysis was conducted to confirm primer specificity, and relative expression levels of *Adra2a* were calculated using the 2^-ΔΔCt method.

Statistical analysis

All experimental data are presented as mean ± standard deviation (x ± s). Statistical analyses were performed using SPSS 26.0, R 4.2.0, and GraphPad Prism 8.0.2 software. Group comparisons were performed using independent sample t-tests (for two groups) or one-way ANOVA (for multiple groups). Mendelian randomization analysis and functional enrichment analysis were considered statistically significant with $P < 0.05$. Cell experiments (CCK8 and qRT-PCR) were performed with three independent replicates to ensure result reliability and reproducibility.

Results

MR validation of the causal link between smoking and myocardial infarction

In the two-sample MR analysis, after applying a P-value threshold for selection and adjusting for confounding factors, 127 single nucleotide polymorphisms (SNPs) were included as instrumental variables. The F-statistics of all genetic instruments ranged from 29.76 to 191.09, exceeding the conventional threshold of 10, and showed no significant correlation with the outcome variable.

To clarify the causal relationship between smoking status and MI, multiple MR methods were employed in this study, using genetic variations as instrumental variables to assess the causal effects of smoking (exposure) on MI (outcome). Figure 1A illustrates the MR analysis framework, clearly demonstrating the causal inference pathway. The MR

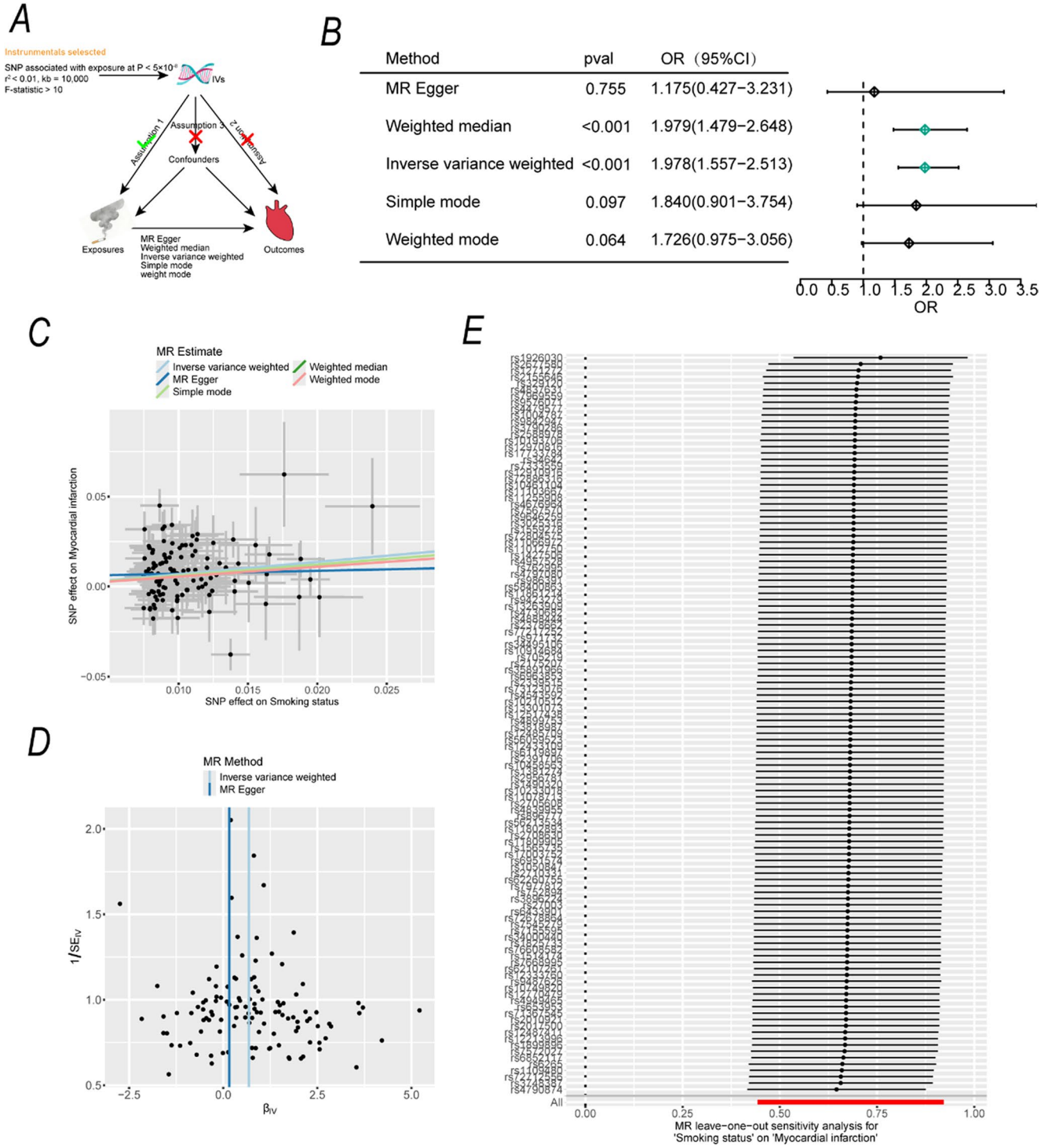

Fig. 1 Two-sample Mendelian randomization (MR) analysis of the association between smoking and myocardial infarction (MI). (**A**) Schematic overview of the MR analysis framework assessing the causal relationship between smoking and MI. (**B**) Forest plot showing effect estimates derived from different MR methods. (**C**) MR scatter plot illustrating the association between smoking-related genetic instruments and MI risk. (**D**) Funnel plot evaluating the distribution of genetic instrumental variable effect estimates. (**E**) Leave-one-out sensitivity analysis assessing the influence of individual SNPs on the overall causal estimate

effect estimate forest plot showed that the inverse variance-weighted method yielded an OR of 1.978 (95% CI = 1.557–2.513, $P < 0.001$), and the weighted median method produced an OR of 1.979 (95% CI = 1.479–2.648, $P < 0.001$). These results indicate a significant positive causal association between smoking and MI in both methods. Additionally, the MR Egger method, the simple model, and the weighted mode method showed positive trends, though not statistically significant, further supporting the association between smoking and an increased MI risk (Fig. 1B). The MR scatter plot further reinforces this association (Fig. 1C). The MR funnel plot demonstrated that the effect estimates of most genetic instrumental variables were symmetrically distributed, and combined with the MR Egger method's P-value (0.755), no significant directional pleiotropy was observed, ensuring the robustness of the results (Fig. 1D).

Sensitivity analysis of MR

To further validate the robustness and reliability of the causal association between smoking and MI, a series of sensitivity analyses were conducted. Cochran's Q test was used to assess heterogeneity among the instrumental variables, with a result of $P = 1.71e\text{-}05$ ($P < 0.05$), indicating significant heterogeneity among the 127 selected SNPs. However, this heterogeneity did not affect the core causal inference.

The MR-Egger intercept test was employed to assess horizontal pleiotropy, revealing an intercept of -0.001920382 ($P = 0.0055$, $P < 0.05$). This suggests the presence of potential horizontal pleiotropy. However, the MR-Egger method itself produced an OR of 1.175 (95% CI = 0.427–3.231), maintaining a consistent positive trend with the IVW method. Furthermore, MR-PRESSO did not identify any outliers among the instrumental variables, with a global test P-value of 0.716 ($P > 0.05$), indicating that the causal effect estimate was not influenced by extreme SNPs (Table 1).

Leave-one-out sensitivity analysis further confirmed the stability of the results. After sequentially removing each SNP, the overall causal effect estimate did not show substantial fluctuations (OR remained close to 1.98), and no single SNP had a dominant impact on the final outcome (Fig. 1E). This suggests that the significant positive causal association between smoking and MI is stable and unaffected by any specific instrumental variable.

Table 1 Sensitivity analyses for the causal association between smoking and myocardial infarction

Pleiotropy				Heterogeneity	
MR Egger		MR-PRESSO		Cochran Q	
egger_intercept	P	RSSobs	P	Q	P
-0.001920382	0.0055	-	0.716	190.69	1.71e-05

Potential targets of nicotine and cotinine

To identify the potential targets of nicotine and its metabolite cotinine, high-throughput target prediction was conducted using four databases. Venn diagrams were used to illustrate the distribution and overlap of target predictions across the databases for both substances. Figure 2A and B display the molecular structures of nicotine and cotinine, visualizing the core compounds of cigarettes and environmental pollutants of interest in this study. The Venn diagram of nicotine target predictions identified 304 potential targets (Fig. 2C), while cotinine's target predictions identified 190 potential targets (Fig. 2D). Further analysis of the overlap between the two substances revealed 97 shared targets, which serve as the core basis for exploring the relationship between cigarette components and MI (Fig. 2E).

Pathway enrichment analysis of nicotine and cotinine targets

To explore the functional and pathway characteristics of nicotine and cotinine targets, GO functional enrichment, KEGG pathway enrichment, and Reactome pathway enrichment analyses were conducted. The GO enrichment analysis covered BP, MF, and CC. In the biological process dimension, targets were predominantly enriched in pathways related to cardiovascular regulation, such as "G-protein coupled receptor signaling," "vascular process in the circulatory system," and "lumen diameter regulation." In the molecular function dimension, the targets were enriched in "neurotransmitter receptor activity" and "G-protein coupled receptor activity." The cellular component dimension focused on "synaptic membrane" and "postsynaptic membrane" (Fig. 3A). KEGG pathway enrichment revealed that targets were primarily enriched in pathways such as "neuroactive ligand-receptor interaction," "calcium signaling," and "cAMP signaling" (Fig. 3B). Reactome pathway enrichment indicated involvement in pathways like "complement system," "inflammatory response," and "apoptosis" (Fig. 3C). These enriched pathways highlight the relevance of nicotine and cotinine targets to cardiovascular regulation and MI pathology, providing direction for subsequent core target selection.

Screening of common targets between nicotine, cotinine, and myocardial infarction, and ppi network and functional characterization

To identify the common targets between nicotine, cotinine, and MI, and analyze their PPI network and functional characteristics, a Venn diagram was first used to screen the overlapping targets. Subsequently, the PPI network was constructed,

and GO functional and KEGG pathway enrichment analyses were performed. The Venn diagram identified 44 overlapping targets from 2,622 MI-related targets and 97 nicotine/cotinine targets (Fig. 4A). The PPI network illustrated interactions among these 44 common targets, with nodes representing individual targets (including ADRA2A, TNF, and ACE) and edges representing protein–protein associations, highlighting ADRA2A and TNF as key hub nodes. GO enrichment revealed cardiovascular-related biological processes including lumen diameter regulation, vascular diameter maintenance, and circulatory system vascular processes, together with molecular functions such as G protein–coupled amine receptor activity and neurotransmitter receptor activity. KEGG analysis highlighted pathways including calcium signaling and neuroactive ligand–receptor interaction, both strongly implicated in cardiovascular homeostasis (Fig. 4B).

Core target selection and transcriptomic validation

To identify key core targets from the common targets between nicotine, cotinine, and MI, and to validate their expression in MI using clinical transcriptomic data, we employed two topological algorithms, MCC and DEGREE, to screen core targets from the PPI network. The intersection of the two algorithms was combined with MI-related transcriptomic data from the GEO database (GSE113871, GSE115031) for expression validation. The MCC algorithm identified key targets such as ADRA2A, SLC6A3, and DRD1, which were located at the core of the network (Fig. 5A). The DEGREE algorithm identified TNF, SLC6A4, SLC6A3, and ADRA2A as key nodes in the network (Fig. 5B). A Venn diagram revealed four core targets common to both algorithms, which may serve as key mediators of the link between cigarette components and MI (Fig. 5C) (Table 2). UMAP dimensionality reduction of the GSE113871 and GSE115031 datasets showed clear clustering between the "Hypoxia" (MI sample) and "Normal" (control sample) groups, indicating good phenotypic distinction and supporting further expression analysis (Fig. 5D and E). Volcano plot analysis of the GSE113871 dataset revealed a significant upregulation of ADRA2A in MI samples (Fig. 5F), and similar results were observed in the GSE115031 dataset (Fig. 5G). These consistent findings across two independent transcriptomic datasets suggest that ADRA2A is a key functional target mediating the relationship between cigarette components and MI.

Molecular docking and molecular dynamics simulations of nicotine, cotinine, and ADRA2A

To assess the potential interaction and binding stability of nicotine, cotinine, and the key target ADRA2A, molecular docking analysis was first performed, followed by molecular dynamics (MD) simulations to evaluate structural stability. In silico molecular docking indicated that nicotine may potentially bind to ADRA2A (PDB ID: 6KUX) with a predicted binding affinity of −7.2 kcal/mol, forming putative hydrogen bonds with THR373 and PHE374 (Fig. 6A). Similarly, as depicted in Fig. 6B, cotinine also showed potential binding to ADRA2A with a predicted affinity of −6.8 kcal/mol, and putative hydrogen bond interactions with SER419, ASP79, and ASP113.

Fig. 2 Molecular structures of nicotine and cotinine and prediction of their potential targets. (**A**) Chemical structure of nicotine. (**B**) Chemical structure of cotinine. (**C**) Venn diagram of predicted nicotine targets based on the SEA, TargetNET, SwissTargetPrediction, and ChEMBL databases. (**D**) Venn diagram of predicted cotinine targets based on the same databases. (**E**) Venn diagram showing shared potential targets of nicotine and cotinine

MD simulation results revealed distinct conformational characteristics of ADRA2A in the apo and ligand-bound states (Table 3). For the nicotine-ADRA2A complex (Fig. 7A), the apo protein (gray line) showed large conformational fluctuations, with RMSD stabilizing at 8–12 Å, while the nicotine-bound complex (red line) rapidly converged and remained stable at 2–5 Å. For the cotinine-ADRA2A complex (Fig. 7G), the apo protein RMSD (gray line) drifted from 8 to 10 Å to 12–13 Å during the simulation, whereas the cotinine-bound complex (red line) remained stable within 2–6 Å. These results demonstrate that both ligands effectively stabilized the overall structure of ADRA2A.

In the nicotine-ADRA2A complex (Fig. 7B), the apo ADRA2A (gray line) exhibited prominent flexibility peaks, particularly at the N-terminal region (residues 0–50) and the intracellular loop regions (residues ~ 150–350), with peak values reaching 6–9 Å. Compared to the apo state, the nicotine-bound ADRA2A (red line) showed significantly reduced RMSF values across most residues, particularly in the range of 250–350, confirming the stabilizing effect of nicotine on protein structure. In the cotinine-ADRA2A complex (Fig. 7H), the RMSF profiles of the apo protein (gray line) and the cotinine-bound complex (red line) were highly similar throughout the entire residue range. No significant difference in flexibility was observed between the two states; both displayed comparable peak fluctuations (approximately 4–6 Å) in the loop regions and low fluctuations in the structured regions. These results indicate that cotinine binding exerts minimal effect on the conformational flexibility of ADRA2A.

In addition, the radius of gyration and solvent-accessible surface area remained relatively stable during the trajectories, supporting the maintenance of compact and well-equilibrated protein-ligand conformations (Fig. 7C, D, I and J). Hydrogen bond analysis revealed persistent intermolecular interactions in both complexes, although the number and temporal distribution of hydrogen bonds differed between the two ligands, reflecting distinct binding

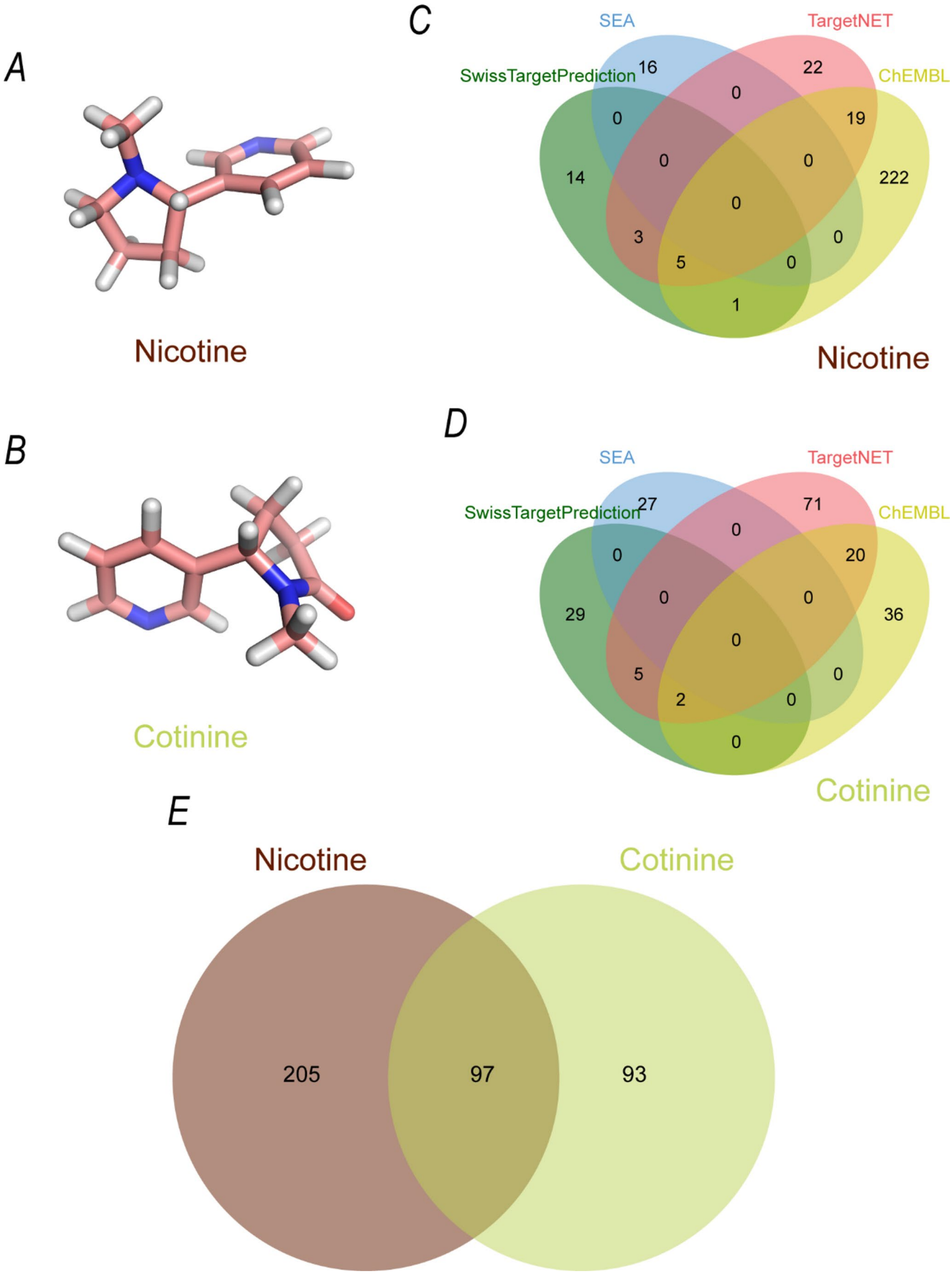
A
Nicotine
B
Cotinine
C
SEA
TargetNET
SwissTargetPrediction
ChEMBL
16
22
0
0
19
0
0
14
0
222
0
3
0
5
0
1
Nicotine
D
SEA
TargetNET
SwissTargetPrediction
ChEMBL
27
71
0
0
20
0
0
29
0
36
0
5
0
2
0
0
Cotinine
E
Nicotine
Cotinine
205
97
93

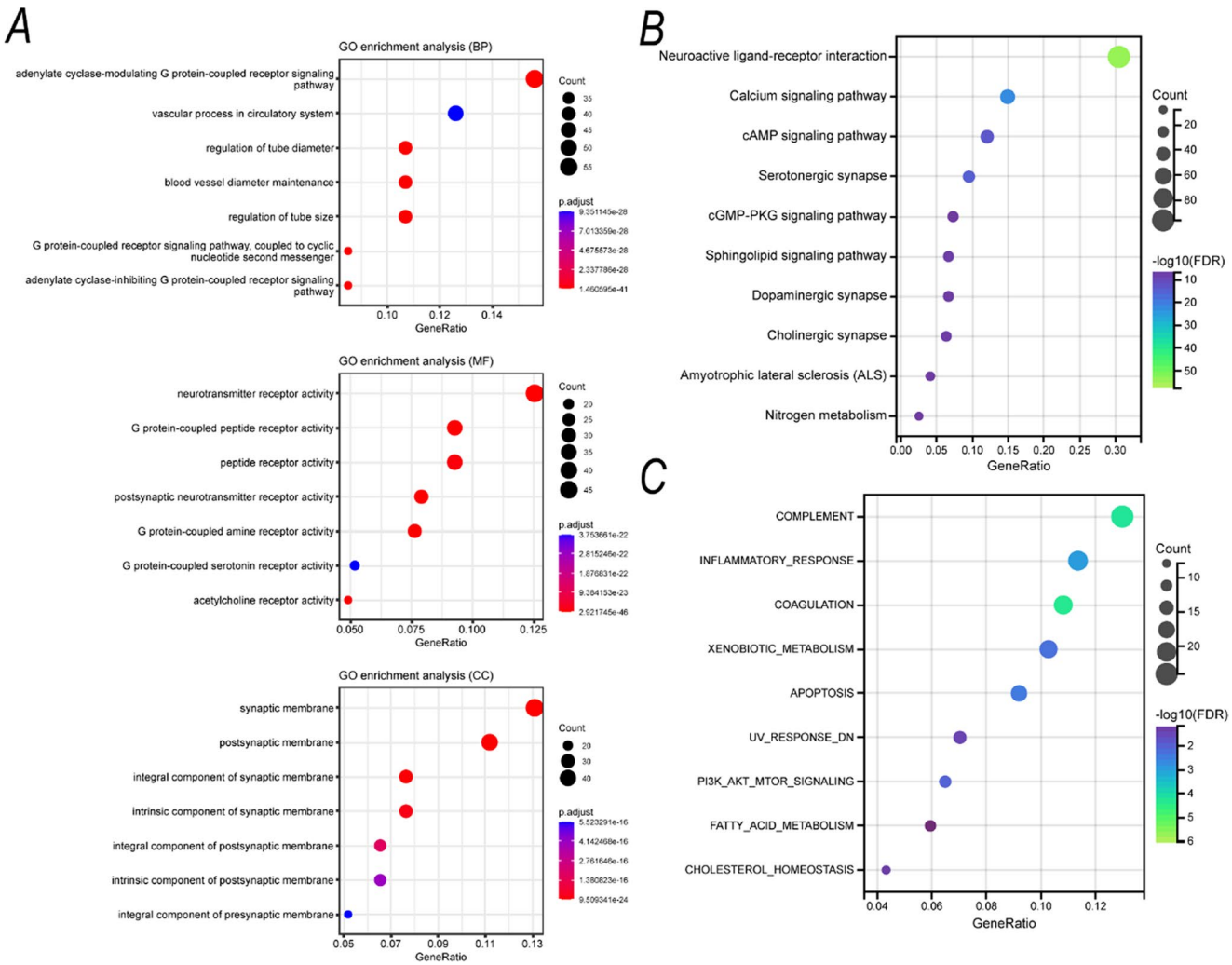

Fig. 3 Functional and pathway enrichment analyses of potential targets of nicotine and cotinine. (**A**) Gene Ontology (GO) enrichment analysis of potential targets, including biological processes (BP), molecular functions (MF), and cellular components (CC). (**B**) KEGG pathway enrichment analysis of potential targets. (**C**) Reactome pathway enrichment analysis of potential targets

modes (Fig. 7E and K). Consistently, the Gibbs free energy landscapes of the two ligand-bound systems displayed well-defined low-energy basins, indicating that both complexes converged toward energetically favorable conformational states (Fig. 7F and L). Collectively, these results support that both small molecules successfully bound to ADRA2A and formed dynamically stable protein-ligand complexes.

In vitro validation of the toxicity of nicotine and cotinine on myocardial cells and their regulation of Adra2a expression

To validate the toxicity of nicotine and cotinine on myocardial cells and their regulatory effects on *Adra2a* expression, H9c2 myocardial cells were treated with varying concentrations of nicotine and cotinine (0, 1, 5, 10, 20, 40, 50, 100, 200 μM) for 72 h. Cell viability was measured using the CCK-8 assay. The results showed that cell viability exhibited an overall decreasing trend with increasing nicotine concentrations (Fig. 8A), with an estimated IC50 of 42.37 μM. Similarly, cotinine treatment also led to an overall decreasing trend in cell viability across the tested concentrations (Fig. 8B), yielding an IC50 of 8.92 μM. qRT-PCR analysis of *Adra2a* mRNA expression revealed that both nicotine and cotinine treatment significantly upregulated *Adra2a* expression compared to the control group ($P<0.05$), with statistically significant effects in both treatment groups (Fig. 8C).

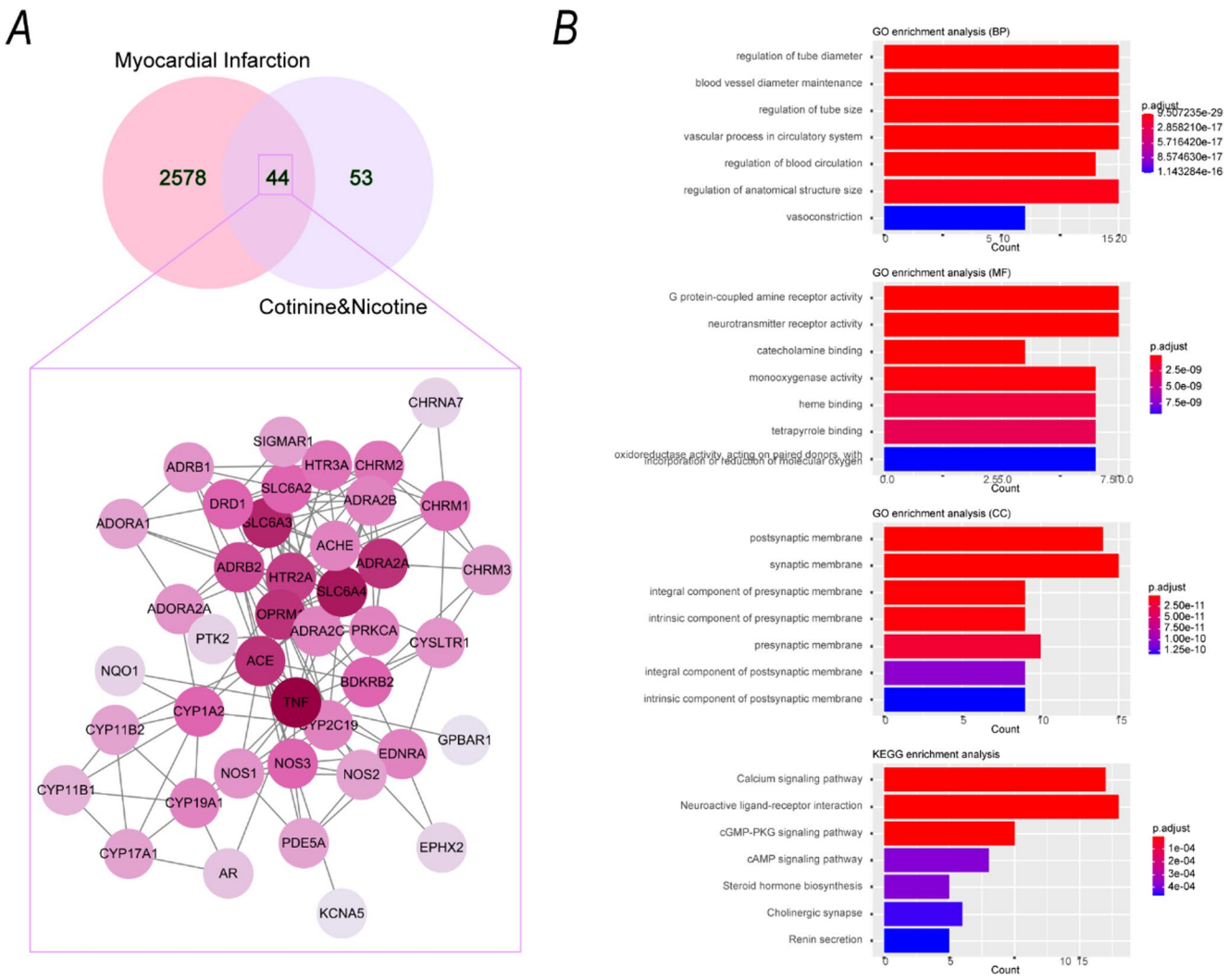

Fig. 4 Protein–protein interaction (PPI) network and functional characterization of shared targets of nicotine, cotinine, and MI. (**A**) PPI network of common targets associated with nicotine, cotinine, and MI, where nodes represent target proteins and edges represent protein–protein interactions. (**B**) GO functional and KEGG pathway enrichment analyses of the shared targets

Discussion

This study employed an integrative, multi-level approach combining Mendelian randomization (MR), network toxicology, molecular docking and dynamics simulations, and in vitro cellular experiments to systematically elucidate the potential molecular mechanisms underlying smoking-associated myocardial infarction (MI). MR analysis, by minimizing confounding and reverse causality, provides genetic evidence supporting a potential causal relationship between smoking and MI. Network toxicology functional enrichment analysis revealed that nicotine and cotinine potential targets were significantly enriched in cardiovascular regulatory pathways (e.g., G protein-coupled receptor signaling and calcium signaling) and MI-related pathological processes, including inflammation and apoptosis. Protein-protein interaction (PPI) network topology analysis identified four core targets, of which only ADRA2A was consistently upregulated in MI samples across two independent GEO transcriptomic datasets (GSE113871 and GSE115031). Molecular docking and dynamics simulations indicated that both nicotine and cotinine are likely to stably bind to the active pocket of ADRA2A through hydrogen bonding and hydrophobic interactions. In vitro experiments further confirmed that nicotine and cotinine reduced H9c2 cardiomyocyte viability in an overall decreasing trend and significantly upregulated ADRA2A mRNA expression. Collectively, these findings support a mechanistic cascade whereby nicotine and cotinine mediate myocardial injury via ADRA2A, thereby identifying ADRA2A as a key functional mediator in smoking-related cardiovascular damage relevant to MI.

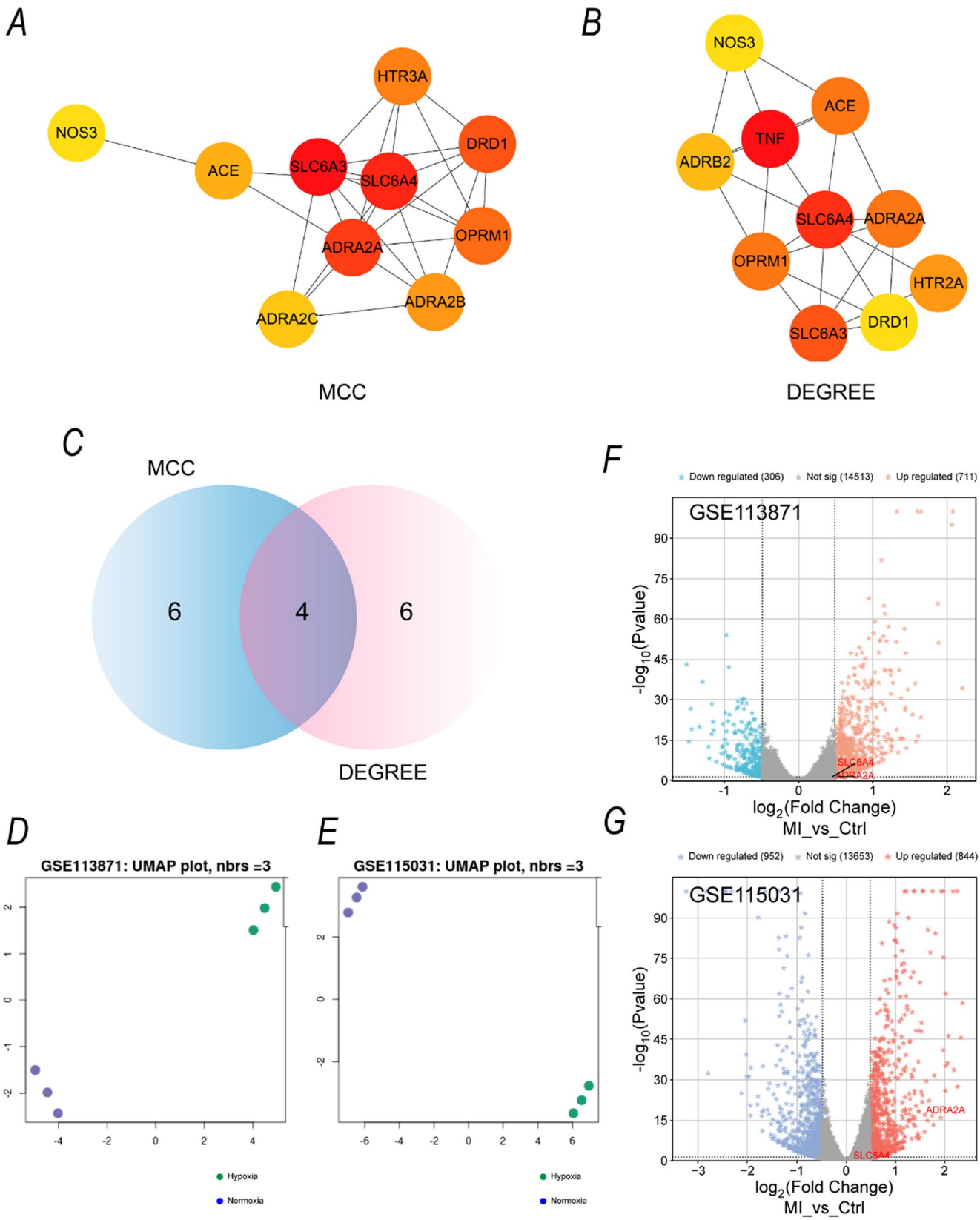
A
HTR3A
NOS3
ACE
SLC6A3
SLC6A4
DRD1
ADRA2A
OPRM1
ADRA2C
ADRA2B
MCC
B
NOS3
ACE
TNF
ADRB2
SLC6A4
ADRA2A
OPRM1
HTR2A
SLC6A3
DRD1
DEGREE
C
MCC
6
4
6
DEGREE
F
Down regulated (306)
Not sig (14513)
Up regulated (711)
GSE113871
-log10(Pvalue)
SLC6A4
ADRA2A
log2(Fold Change)
MI_vs_Ctrl
D
GSE113871: UMAP plot, nbrs =3
Hypoxia
Normoxia
E
GSE115031: UMAP plot, nbrs =3
Hypoxia
Normoxia
G
Down regulated (952)
Not sig (13653)
Up regulated (844)
GSE115031
-log10(Pvalue)
ADRA2A
SLC6A4
log2(Fold Change)
MI_vs_Ctrl

Fig. 5 Identification of hub targets and transcriptomic validation. (**A**) Hub targets identified from the PPI network using the Maximal Clique Centrality (MCC) algorithm. (**B**) Hub targets identified using the Degree algorithm. (**C**) Venn diagram showing overlapping hub targets identified by the MCC and Degree algorithms. (**D**) UMAP dimensionality reduction plot of the GSE113871 dataset showing clustering of hypoxia-treated (MI) and control samples. (**E**) UMAP dimensionality reduction plot of the GSE115031 dataset. (**F**) Volcano plot of differentially expressed genes (DEGs) between MI and control samples in the GSE113871 dataset. (**G**) Volcano plot of DEGs in the GSE115031 dataset

MR, as a genetic variant-based causal inference method, effectively mitigates confounding biases inherent to observational studies of smoking and MI (e.g., co-exposures such as alcohol consumption or obesity) and addresses reverse causation (e.g., behavioral changes following MI onset) (Jabeen et al. 2025, Benn et al. 2012). In this study, both inverse variance weighted (IVW) and weighted median analyses demonstrated a significant positive causal effect of smoking on increased MI risk. Although MR-Egger intercept testing suggested potential horizontal pleiotropy ($P < 0.05$), no outlier SNPs were detected by MR-PRESSO. Leave-one-out analysis and funnel plots further supported the robustness of the causal association. Consistency of effect estimates across multiple MR methods further reduced the likelihood that pleiotropy substantially biased the primary conclusion. These results were consistent with previous findings by Gao et al. (2025), and further support the public health relevance of smoking as a modifiable risk factor for MI, while providing genetic evidence highlighting the importance of smoking prevention in primary cardiovascular disease prevention. As nicotine and cotinine are the most abundant and biologically stable active constituents in tobacco smoke, investigating their specific molecular targets and mechanisms provides a targeted, component-based strategy for dissecting the pathways underlying smoking-related myocardial injury.

ADRA2A, a member of the adrenergic receptor family, is predominantly expressed in vascular smooth muscle cells, cardiomyocytes, and nerve terminals. It regulates vascular tone, myocardial contractility, and neurotransmitter release via cAMP and calcium signaling pathways (Zhou et al. 2025, Kurnik et al. 2006). Previous studies have demonstrated that α2-adrenergic receptors, including ADRA2A, exert cardioprotective effects under physiological conditions by suppressing excessive sympathetic activity and reducing oxidative stress injury (Jarrar et al. 2022). However, under pathological conditions such as nicotine exposure, these receptors are prone to severe desensitization or overactivation, which inactivates downstream protective signaling pathways and exacerbates cardiomyocyte injury (Calvo et al. 2024).

Table 2 Topological scores of core targets for nicotine, cotinine, and myocardial infarction identified by MCC and degree algorithms

node_name	MCC	node_name	Degree
SLC6A3	246	TNF	17
SLC6A4	238	SLC6A4	15
ADRA2A	228	SLC6A3	14
DRD1	181	ADRA2A	13
OPRM1	172	OPRM1	13
HTR3A	132	ACE	13

At the human clinical level, the association between smoking and systemic oxidative stress has been confirmed by multiple studies. Kumari et al. found that among patients following MI, smokers exhibited a significantly greater decrease in antioxidant enzyme activity and a greater increase in lipid peroxidation than non-smokers, suggesting that smoking amplifies post-MI myocardial injury by exacerbating oxidative stress (Sathiyaraj et al. 1997). Of note, ADRA2A exerts its cardioprotective effects under physiological conditions precisely by mitigating oxidative stress (Jarrar et al. 2022). The persistent oxidative stress state induced by smoking (and nicotine exposure) may directly challenge the protective functional reserve of ADRA2A, rendering it more susceptible to desensitization or functional impairment, thereby weakening myocardial defense against oxidative damage (Calvo et al. 2024).

Furthermore, genetic variants of the ADRA2A gene are directly associated with cardiovascular clinical phenotypes in humans. Song et al., in a clinical study of 1,024 Chinese patients undergoing percutaneous coronary intervention (PCI), found that ADRA2A single nucleotide polymorphisms (SNPs) rs11195419 and rs3750625 were significantly associated with adenosine diphosphate (ADP)-induced platelet aggregation, and this effect was more pronounced in male patients (Song et al. 2017). Another study reported that the ADRA2A -1291 C>G polymorphism, in combination with variants of other catecholamine system genes, was significantly associated with the risk of cardiovascular dysfunction in adolescents with essential hypertension (Kosovtseva et al. 2019). These genetic findings suggest that ADRA2A variants may participate in the clinical phenotype spectrum of coronary artery disease and myocardial infarction through the regulation of platelet activation and vasomotor function. Together with the smoking-induced oxidative stress environment, these observations imply that individuals carrying ADRA2A genetic variants may be more susceptible to nicotine-induced cardiovascular injury.

Importantly, as nicotine and cotinine are persistent environmental pollutants present in thirdhand smoke, even low-level but chronic exposure may be sufficient to subtly yet continuously perturb ADRA2A conformation and signaling. Our findings raise the possibility that such environmentally relevant exposure levels, over time, could

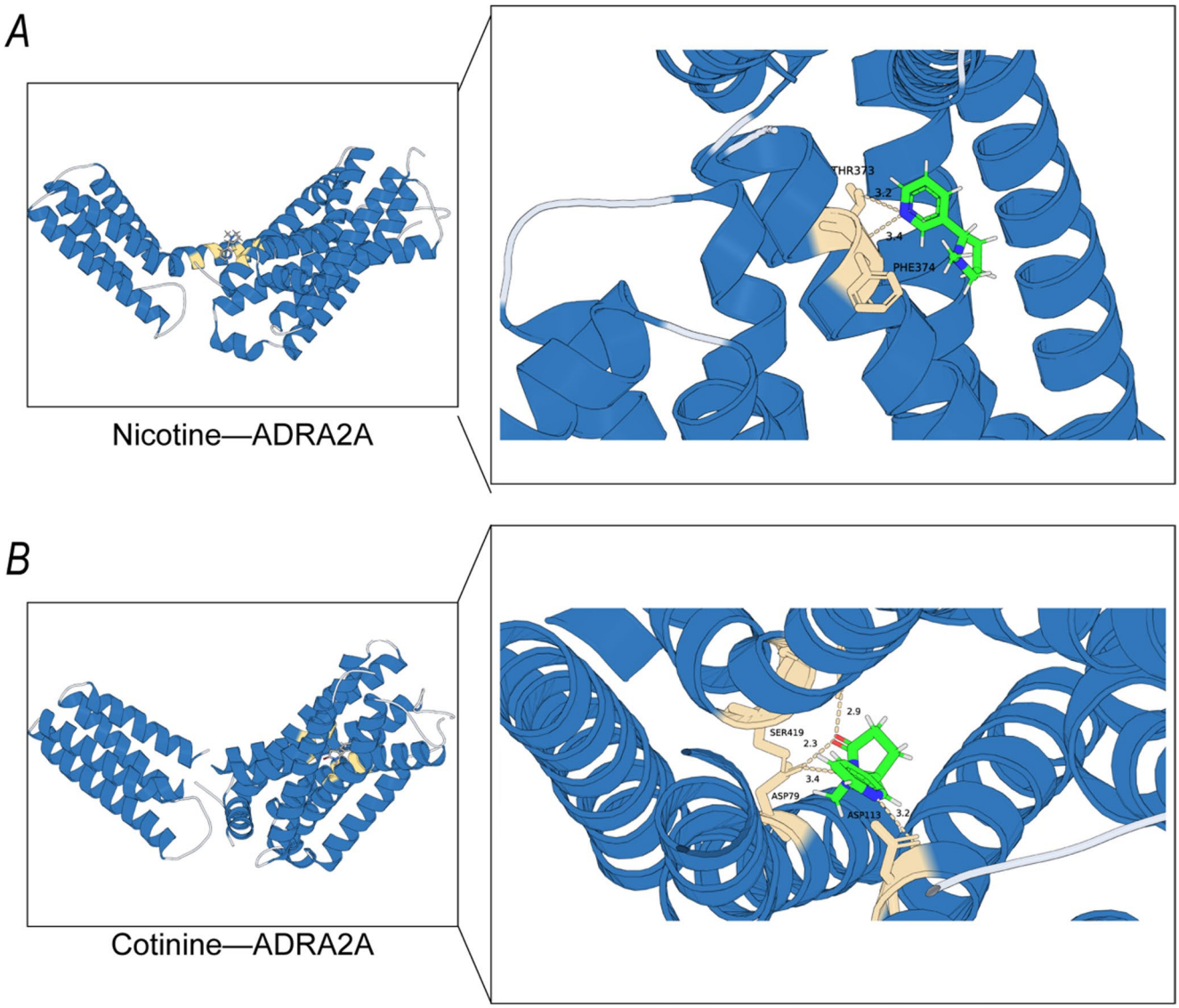

Fig. 6 Molecular docking models of nicotine and cotinine with ADRA2A. (**A**) Binding mode of nicotine with the ADRA2A protein. (**B**) Binding mode of cotinine with the ADRA2A protein

Table 3 Summary of molecular dynamics simulation metrics for ADRA2A systems

		RMSD	RMSF	Rg	SASA	H-bonds
ADRA2A without Nocotine	min	0	0.762	25.1333	19570.2303	-
	max	13.651	8.969	28.12107	22092.13224	-
	mean	8.965271864	2.627244949	26.14759254	20634.43235	-
ADRA2A with Nocotine	min	0	0.795	26.7018	20084.41829	0
	max	5.4	7.126	30.26327	22357.33422	3
	mean	3.77287956	1.901901515	28.86074006	21115.42358	0.792603698
ADRA2A without Cotinine	min	0	0.718	26.65247	19237.10478	-
	max	13.311	7.567	29.89089	21382.00958	-
	mean	10.92383558	2.353393939	28.14669606	21227.55388	-
ADRA2A with Cotinine	min	0	0.661	25.7545	19695.51017	0
	max	6.495	8.552	29.48531	21978.81282	3
	mean	3.312327836	2.162179293	27.64634218	21150.32602	1.418290855

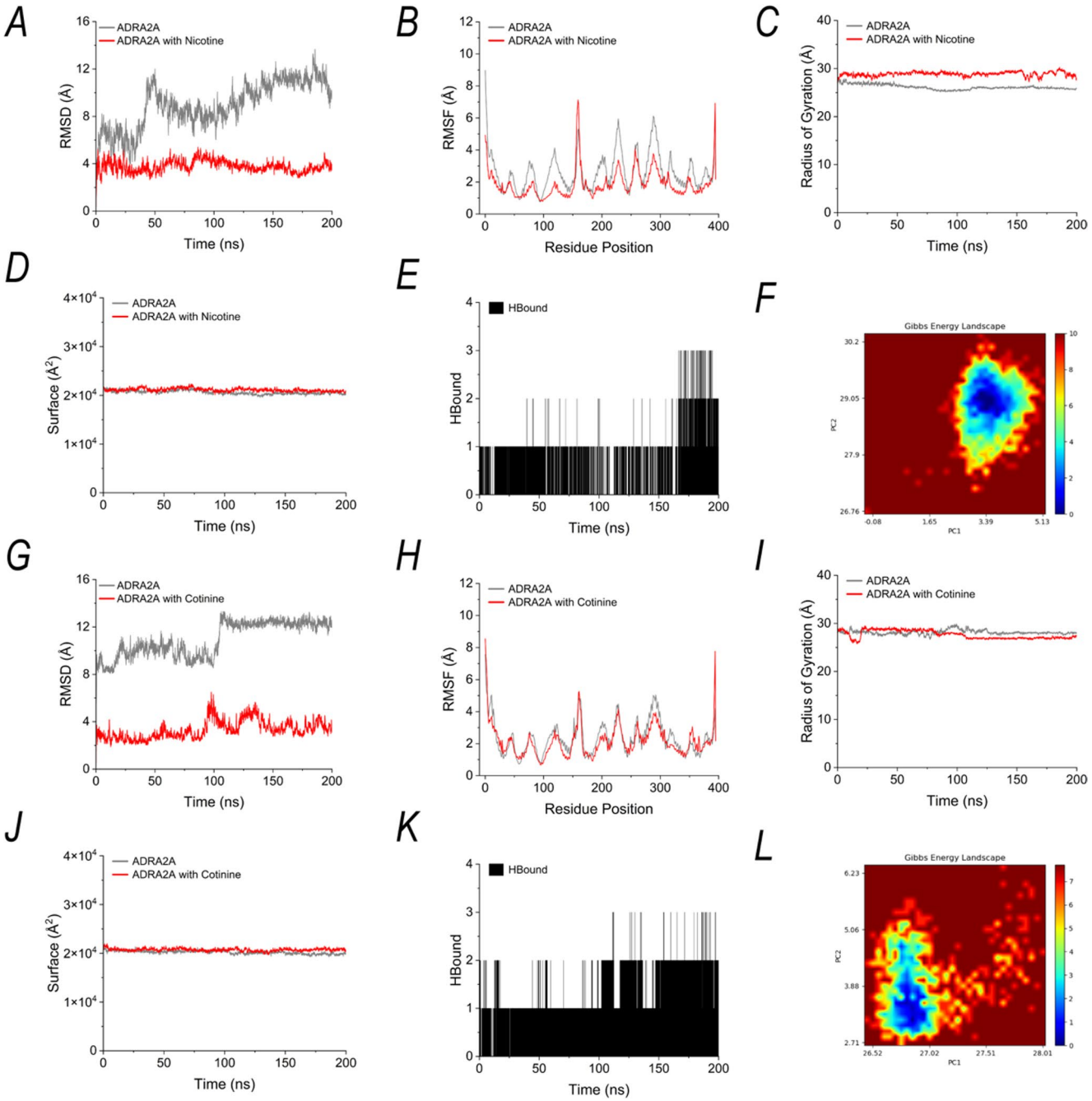

Fig. 7 Molecular dynamics (MD) simulation results of nicotine–ADRA2A and cotinine–ADRA2A complexes. (**A**) Root mean square deviation (RMSD) of the nicotine–ADRA2A complex. (**B**) Root mean square fluctuation (RMSF) of ADRA2A residues in the nicotine–ADRA2A complex. (**C**) Radius of gyration (Rg) of the nicotine–ADRA2A complex. (**D**) Solvent-accessible surface area (SASA) of the nicotine–ADRA2A complex. (**E**) Number of hydrogen bonds in the nicotine–ADRA2A complex. (**F**) Gibbs free energy landscape (GEL) of the nicotine–ADRA2A complex. (**G**) RMSD of the cotinine–ADRA2A complex. (**H**) RMSF of ADRA2A residues in the cotinine–ADRA2A complex. (**I**) Radius of gyration of the cotinine–ADRA2A complex. (**J**) SASA of the cotinine–ADRA2A complex. (**K**) Number of hydrogen bonds in the cotinine–ADRA2A complex. (**L**) GEL of the cotinine–ADRA2A complex

recapitulate the same pathological transition—from compensatory ADRA2A upregulation to functional impairment—observed in our in vitro model, thereby contributing to myocardial infarction risk in non-smoking populations exposed to thirdhand smoke.

In the present study, ADRA2A expression was significantly upregulated in two independent myocardial infarction transcriptomic datasets, suggesting that ADRA2A may represent a stress-induced compensatory response during MI, attempting to attenuate injury by inhibiting excessive

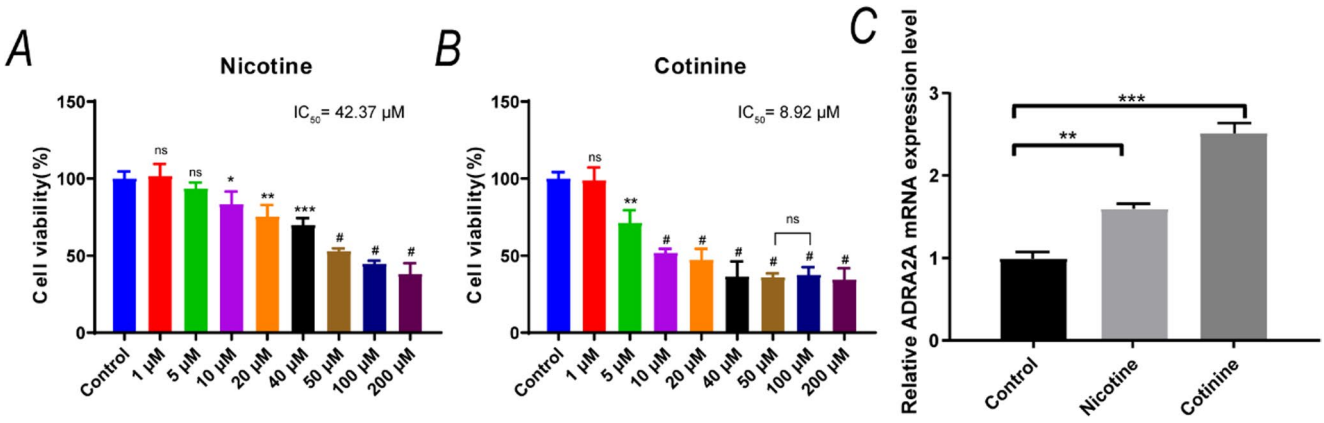

Fig. 8 Cytotoxic effects of nicotine and cotinine on H9c2 cardiomyocytes and regulation of *Adra2a* expression. (**A**) Cell viability of H9c2 cells after 72 h exposure to different concentrations of nicotine, assessed by CCK-8 assay. (**B**) Cell viability of H9c2 cells after 72 h exposure to different concentrations of cotinine. (**C**) *Adra2a* mRNA expression levels in H9c2 cells following nicotine and cotinine treatment, measured by qRT-PCR

sympathetic outflow. However, our in vitro experiments showed that nicotine and cotinine significantly upregulated ADRA2A expression while reducing cardiomyocyte viability, indicating that under nicotine exposure, this upregulation exceeds the range of physiological compensation and transitions into a pathological stress response. Molecular docking and molecular dynamics simulations predicted that nicotine and cotinine may interact with the ADRA2A, potentially influencing the dynamic conformation of the receptor through hydrogen bonding. This interaction may interfere with the normal signal transduction function of the receptor, thereby contributing to the regulation of myocardial injury.

Collectively, these findings indicate that the upregulation of ADRA2A induced by nicotine and cotinine is not an enhancement of the compensatory protective mechanism, but a key step in promoting cardiomyocyte injury, which is fully consistent with the observed reduction in cell viability. Furthermore, as a key mediator in various disease processes, ADRA2A has been recognized as an important therapeutic target, and selective antagonists have been developed as pharmacological tools to study its roles in inflammation and cardiovascular diseases (Chayka et al. 2024). This study, combining cellular experiments and computational simulations, provides new theoretical clues regarding the potential interaction between nicotine/cotinine and ADRA2A and its pathological role in smoking-related myocardial infarction, laying a foundation for the development of subsequent targeted intervention strategies.

However, we acknowledge that the current data are insufficient to directly determine whether nicotine and cotinine act as agonists, antagonists, or allosteric modulators of ADRA2A. Molecular docking and dynamics simulations can reveal binding modes and conformational stability but cannot assign functional classification, which requires functional assays. The observed upregulation of ADRA2A mRNA is more consistent with a compensatory response often seen after receptor inhibition (e.g., by an antagonist), whereas prolonged exposure to a typical agonist usually induces receptor downregulation. Del Calvo et al. (2024) demonstrated that nicotine induces severe desensitization of ADRA2A and attenuates agonist-mediated cardioprotection against oxidative stress (Calvo et al. 2024); however, that study did not directly clarify nicotine's own mode of action. Therefore, definitive classification—whether nicotine/cotinine act as antagonists, negative allosteric modulators, or weak partial agonists—requires dedicated functional experiments.

Several limitations should be acknowledged. First, Mendelian randomization (MR) analysis only established the causal association between smoking behavior and myocardial infarction, without directly evaluating the specific genetic causal effects of nicotine or cotinine. Additionally, a significant MR-Egger intercept suggests potential horizontal pleiotropy; moreover, the analysis relies on GWAS data from European populations, and the results may not be directly generalizable to other ethnic groups due to genetic heterogeneity. Second, the GEO transcriptomic dataset used for validation has a small sample size, which may reduce the statistical power of differential expression analysis. Third, the in vitro experiments were conducted using rat-derived H9c2 cardiomyocytes rather than human primary cardiomyocytes, while the computational models were based on the human ADRA2A structure. Although human and rat ADRA2A share 91.18% amino acid sequence identity, potential species-specific differences in receptor conformation or signaling cannot be completely excluded. Additionally, the concentrations of nicotine and cotinine used (especially in high-dose groups) may exceed physiological exposure levels in humans. Therefore, the functional relevance of the 'nicotine-ADRA2A-myocardial infarction' regulatory axis requires further validation using human

cardiomyocytes (e.g., iPSC-derived) and in vivo models. Finally, the direct association between the compounds and the target is solely based on molecular docking and simulation results, lacking experimental validation at the bench-top level, such as surface plasmon resonance (SPR) and isothermal titration calorimetry (ITC) assays.

Future research should focus on: (1) establishing MI animal models combining smoking exposure with ADRA2A knockdown or overexpression to validate its causal role in vivo; (2) conducting clinical cohort studies to assess ADRA2A expression in peripheral blood and myocardial tissue from smoking and non-smoking MI patients, correlating expression with disease severity and prognosis; (3) identifying ADRA2A-specific inhibitors or antagonistic peptides and evaluating their therapeutic potential in smoking-associated MI; and (4) applying single-cell sequencing to elucidate ADRA2A expression and regulation across distinct cardiomyocyte subpopulations.

In conclusion, through a multidisciplinary integrative approach, this study systematically demonstrates that ADRA2A is a critical mediator of nicotine- and cotinine-induced MI, revealing the molecular mechanism of the "smoking–nicotine/cotinine–ADRA2A–cardiomyocyte injury" axis and providing novel insights and potential therapeutic targets for the prevention and treatment of smoking-related cardiovascular disease.

Author contributions Yang Fu supervised the project, provided funding and wrote the initial draft. Chen Liu performed bioinformatics analysis. Lifang Su assisted with visualization and revisions.

Funding Medical Science Research Project of Hebei Province [20250062].

Data availability The GEO public datasets used in this study and available in the data repository have the following accession number GSE113871 and GSE115031 microarray data.

Declarations

Ethics, consent to participate, and consent to publish Not applicable.

Clinical trial number Not applicable.

Competing interests The authors declare no competing interests.

References

Balakumar P, Kaur J (2009) Is nicotine a key player or spectator in the induction and progression of cardiovascular disorders? Pharmacol Res 60(5):361–368

Baykan A, Narin N, Narin F, Akgün H, Yavaşcan S, Saraymen R (2008) The protective effect of melatonin on nicotine-induced myocardial injury in newborn rats whose mothers received nicotine. Anadolu Kardiyol Derg 8(4):243–248

Benn M, Tybjaerg-Hansen A, McCarthy MI, Jensen GB, Grande P, Nordestgaard BG (2012) Nonfasting glucose, ischemic heart disease, and myocardial infarction: a Mendelian randomization study. J Am Coll Cardiol 59(25):2356–2365

Bowden J, Davey Smith G, Burgess S (2015) Mendelian randomization with invalid instruments: effect estimation and bias detection through Egger regression. Int J Epidemiol 44(2):512–525

Bowden J, Davey Smith G, Haycock PC, Burgess S (2016) Consistent Estimation in Mendelian Randomization with Some Invalid Instruments Using a Weighted Median Estimator. Genet Epidemiol 40(4):304–314

Bujnova K, Barta A, Lakota J, Cebova M (2025) Impact of High-Fat Diet on Biochemical Changes Following Experimental Myocardial Infarction. J Cell Mol Med 29(23):e70984

Chayka A, Česnek M, Kužmová E, Kozák J, Tloušťová E, Dvořáková A, Strmeň T, Brož B, Osifová Z, Dračínský M et al (2024) Structure-Based Drug Design of ADRA2A Antagonists Derived from Yohimbine. J Med Chem 67(12):10135–10151

Chen X, Kong J, Diao X, Cai J, Zheng J, Xie W, Qin H, Huang J, Lin T (2020) Depression and prostate cancer risk: A Mendelian randomization study. Cancer Med 9(23):9160–9167

Cheng W, Lin P, Yang Z, Xie Y, Gao D, Chen M (2026) A new perspective on the neurotoxic mechanisms of six typical per- and polyfluoroalkyl substances (PFAS): insights from integrating network toxicology and random forest algorithm. Drug Chem Toxicol 49(1):130–148

Cojocaru PA, Țieranu ML, Piorescu MTL, Buciu IC, Belu AM, Cureraru SI, Țieranu EN, Moise GC, Istratoaie O (2025) Myocardical infarction in young adults: revisiting risk factors and atherothrombotic pathways. Med (Kaunas) 61(9):1615

Corbin LJ, Richmond RC, Wade KH, Burgess S, Bowden J, Smith GD, Timpson NJ (2016) BMI as a Modifiable Risk Factor for Type 2 Diabetes: Refining and Understanding Causal Estimates Using Mendelian Randomization. Diabetes 65(10):3002–3007

Dasgupta S (2024) Identification and molecular modelling of potential drugs targeting the genes involved in the progression of lung cancer in patients with idiopathic pulmonary fibrosis. Gene Rep 37:102067

Del Calvo G, Pollard CM, Baggio Lopez T, Borges JI, Suster MS, Lymperopoulos A (2024) Nicotine Diminishes Alpha2-Adrenergic Receptor-Dependent Protection Against Oxidative Stress in H9c2 Cardiomyocytes. Drug Des Devel Ther 18:71–80

Del Calvo G, Pollard CM, Baggio Lopez T, Borges JI, Suster MS, Lymperopoulos A (2024) Nicotine diminishes alpha2-adrenergic receptor-dependent protection against oxidative stress in H9c2 cardiomyocytes. Drug Des Devel Ther 18:71–80

Gao S, Huang S, Liu X, Yu M, Zhao L (2025) Impact of smoking cessation on cardiovascular outcomes in patients with myocardial infarction with nonobstructive coronary arteries. Am J Prev Cardiol 23:101080

Ghanem L, Moubarak A, Kotaich J, Mouannes M, Ghanem A, Chamat S, Bitar N (2026) Evaluating cancer risks: The impact of third-hand smoke exposure on carcinogenesis. Regul Toxicol Pharmacol 164:105991

Greco MF, Minelli C, Sheehan NA, Thompson JR (2015) Detecting pleiotropy in Mendelian randomisation studies with summary data and a continuous outcome. Stat Med 34(21):2926–2940

Hanna ST (2006) Nicotine effect on cardiovascular system and ion channels. J Cardiovasc Pharmacol 47(3):348–358

Hu H, Nakagawa T, Honda T, Yamamoto S, Okazaki H, Ide H, Dohi S, Miyamoto T, Yamamoto M, Gommori N et al (2025) Joint impact of smoking and metabolic syndrome on cardiovascular disease: a cohort study. J Atheroscler Thromb 33(2):181–194

Jabeen T, Todd E, Gauci S, Wootton RE, Marx W, Ashtree DN, Zhang DJ, West E, Davoodian N, Bastawy EM et al (2025) Genetic susceptibility to depression and risk of cardiometabolic diseases: a systematic review and meta-analysis of 21 Mendelian randomisation studies. EClinicalMedicine 89:103587

Jarrar YB, Jarrar Q, Abaalkhail SJ, Moh'd Kalloush H, Naser W, Zihlif M, Al Shhab M, El Madani A, Jamous Y, Lee SJ (2022) Molecular toxicological alterations in the mouse hearts induced by sub-chronic thiazolidinedione drugs administration. Fundam Clin Pharmacol 36(1):143–149

Jia G, Meng Z, Liu C, Ma X, Gao J, Liu J, Guo R, Yan Z, Christopher T, Lopez B et al (2020) Nicotine induces cardiac toxicity through blocking mitophagic clearance in young adult rat. Life Sci 257:118084

Johansson E, Stenman M, Hansson EC, Malm CJ, Perrotta S, Pivodic A, Jeppsson A, Nielsen SJ (2025) Smoking and long-term risks for morbidity and mortality after coronary artery bypass grafting. Int J Cardiol Cardiovasc Risk Prev 27:200512

Khanna AK, Xu J, Mehra MR (2012) Antioxidant N-acetyl cysteine reverses cigarette smoke-induced myocardial infarction by inhibiting inflammation and oxidative stress in a rat model. Lab Invest 92(2):224–235

Klein J, Diaba-Nuhoho P, Giebe S, Brunssen C, Morawietz H (2023) Regulation of endothelial function by cigarette smoke and next-generation tobacco and nicotine products. Pflugers Arch 475(7):835–844

Kosovtseva AS, Bairova TA, Rychkova LV, Polyakov VM, Kolesnikova LI (2019) Prognostic Risk Models for the Development of Cardiovascular Dysfunction in Adolescents with Essential Hypertension. Bull Exp Biol Med 166(4):494–496

Kumar A, Biswas UK (2011) Smoking is associated with reduced serum paraoxonase, antioxidants and increased oxidative stress in normolipidaemic acute myocardial infarct patients. Heart Asia 3(1):115–119

Kurnik D, Muszkat M, Li C, Sofowora GG, Solus J, Xie HG, Harris PA, Jiang L, McMunn C, Ihrie P et al (2006) Variations in the alpha2A-adrenergic receptor gene and their functional effects. Clin Pharmacol Ther 79(3):173–185

La Rosa GRM, Yu J, Geraci G, Capodanno D, Ohki T, George J, Polosa R (2025) Vascular and Cardiovascular Outcomes of Smoking Cessation and Switching to Electronic Cigarette Use: Protocol for a Systematic Review of Prospective Studies. JMIR Res Protoc 14:e74949

Lee SH, Yun SJ, Ryu S, Choi SW, Kim HJ, Kang TK, Oh SC, Cho SJ (2017) Taking varenicline for smoking cessation: a rare cause of pulmonary thromboembolism with infarction. Am J Emerg Med 35(7):1037.e1033-1037.e1036

Liu T, Yang F (2025) Galectin-3 in acute myocardial infarction: from molecular mechanisms to clinical translation. Front Mol Biosci 12:1730173

Lou Y, Jiang F, Guan J (2024) The effect of lipidomes on the risk of endometrioid endometrial cancer: a Mendelian randomization study. Front Oncol 14:1436955

Meng TT, Wang W, Meng FL, Wang SY, Wu HH, Chen JM, Zheng Y, Wang GX, Zhang MX, Li Y et al (2021) Nicotine Causes Mitochondrial Dynamics Imbalance and Apoptosis Through ROS Mediated Mitophagy Impairment in Cardiomyocytes. Front Physiol 12:650055

Nowotka MM, Gaulton A, Mendez D, Bento AP, Hersey A, Leach A (2017) Using ChEMBL web services for building applications and data processing workflows relevant to drug discovery. Expert Opin Drug Discov 12(8):757–767

Ockene IS, Miller NH (1997) Cigarette smoking, cardiovascular disease, and stroke: a statement for healthcare professionals from the American Heart Association. American Heart Association Task Force on Risk Reduction. Circulation 96(9):3243–3247

Patil SS, Bozack AK, Pillarisetti A, Patil SS, Steenland K, Balakrishnan K, Waller LA, Jabbarzadeh S, Peel J, Clasen TF et al (2025) Early-life exposure to secondhand smoke and polycyclic aromatic hydrocarbons: associations with epigenetic aging among children. Environ Epigenet 11(1):dvaf030

Ramalingam A, Budin SB, Mohd Fauzi N, Ritchie RH, Zainalabidin S (2021) Targeting mitochondrial reactive oxygen species-mediated oxidative stress attenuates nicotine-induced cardiac remodeling and dysfunction. Sci Rep 11(1):13845

Rao T, Tong H, Li J, Huang J, Yin Y, Zhang J (2024) Exploring the role and mechanism of hyperoside against cardiomyocyte injury in mice with myocardial infarction based on JAK2/STAT3 signaling pathway. Phytomedicine 128:155319

Riederer AM, Sherris AR, Szpiro AA, Melough MM, Simpson CD, Loftus CT, Day DB, Wallace ER, Trasande L, Barrett ES et al (2025) Environmental and dietary factors associated with urinary OH-PAHs in mid-pregnancy in a large multi-site study. Environ Res 266:120516

Sahin C, Tuncerler G, Bese SA, Ozdel P, Bas R, Torer N, Cevik O, Seyhan NA, Erge D, Uysal P (2026) Cord blood biomarkers predict neonatal respiratory dysfunction after prenatal smoke exposure: A decision tree model. Pediatr Allergy Immunol 37(1):e70271

Sanderson E, Glymour MM, Holmes MV, Kang H, Morrison J, Munafò MR, Palmer T, Schooling CM, Wallace C, Zhao Q et al (2022) Mendelian randomization. Nat Rev Methods Primers 2:6

Sasco AJ, Secretan MB, Straif K (2004) Tobacco smoking and cancer: a brief review of recent epidemiological evidence. Lung Cancer 45(Suppl 2):S3–9

Sathiyaraj D, Muthu R, Mohamed AJ (1997) Antioxidant Status, Proinflammatory Cytokines, and Acute-Phase Protein Response in Smokers after Myocardial Infarction. J Clin Biochem Nutr 22(2):131–137

Song Y, Tang XF, Yao Y, He C, Xu JJ, Wang HH, Gao Z, Wang M, Yuan JQ (2017) Association of α2A-Adrenergic Receptor Genetic Variants with Platelet Reactivity in Chinese Patients on Dual Antiplatelet Therapy Undergoing Percutaneous Coronary Intervention. Biomed Environ Sci 30(12):898–906

Sridharan MR, Flowers NC, Hand RC, Hand JW, Horan LG (1985) Effect of various regimens of chronic and acute nicotine exposure on myocardial infarct size in the dog. Am J Cardiol 55(11):1407–1411

Stelzer G, Rosen N, Plaschkes I, Zimmerman S, Twik M, Fishilevich S, Stein TI, Nudel R, Lieder I, Mazor Y et al (2016) The GeneCards suite: from gene data mining to disease genome sequence analyses. Curr Protoc Bioinformatics 54:1.30.31–31.30.33

Szklarczyk D, Santos A, von Mering C, Jensen LJ, Bork P, Kuhn M (2015) STITCH 5: augmenting protein–chemical interaction networks with tissue and affinity data. Nucleic Acids Res 44(D1):D380–D384

Verbanck M, Chen CY, Neale B, Do R (2018) Detection of widespread horizontal pleiotropy in causal relationships inferred from Mendelian randomization between complex traits and diseases. Nat Genet 50(5):693–698

Wu YT, Zhang GY, Hua Y, Fan HJ, Han X, Xu HL, Chen GH, Liu B, Xie LP, Zhou YC (2023) Ferrostatin-1 suppresses cardiomyocyte ferroptosis after myocardial infarction by activating Nrf2 signaling. J Pharm Pharmacol 75(11):1467–1477

Yao ZJ, Dong J, Che YJ, Zhu MF, Wen M, Wang NN, Wang S, Lu AP, Cao DS (2016) TargetNet: a web service for predicting potential drug-target interaction profiling via multi-target SAR models. J Comput Aided Mol Des 30(5):413–424

Yathindra MR, Odero GO, Govindu SS, Sharma R, Sato K, Mettu TR, Mahorkar AV (2025) Evaluating the Association Between Current Smokers and Myocardial Infarction: A Cross-Sectional Study. Cureus 17(8):e90565

Yuan Z, Lv G, Liu X, Xiao Y, Tan Y, Zhu Y (2025) Machine learning selection of basement membrane-associated genes and development of a predictive model for kidney fibrosis. Sci Rep 15(1):6567

Zhou F, Cai J, Chen L, Tan X, Li C (2025) ADRA2A contributes to airway inflammation and apoptosis in asthma through the ERK signaling in vitro and in vivo. J Inflamm (Lond) 22(1):55